SUPERSONIC WING DESIGN CONCEPTS EMPLOYING NONLINEAR FLOWS

David S. Miller
NASA Langley Research Center
Hampton, Virginia

Abstract

Three nonlinear flow concepts for the design of supersonic wings are reviewed. The specific concepts are: leading-edge thrust, supercritical crossflow, and leading-edge vortex flow. The major results of the experimental-theoretical studies supporting the development of these concepts are presented and discussed. Also, supporting aerodynamic prediction methods are described and example applications are given. Recommendations for further development of each concept are made.

Nomenclature

b	wing span
c	local wing chord
c_r	wing root chord
C_A	wing axial or chord force coefficient
ΔC_A	incremental change in C_A from $\alpha = 0$
C_D	drag coefficient
ΔC_D	drag-due-to-lift coefficient
$C_{D,O}$	drag coefficient at zero lift
C_L	lift coefficient
$C_{L,cru}$	cruise-lift coefficient
$C_{L,des}$	design-lift coefficient
$C_{N,L}$	normal-force coefficient due to wing lower-surface pressures
$C_{N,U}$	normal-force coefficient due to wing upper-surface pressures
C_p	pressure coefficient
ΔC_p	net wing loading coefficient
$C_{p,v}$	vacuum pressure coefficient, $-2/\gamma M^2$
C_t	wing section thrust coefficient
$\bar{C}_t$	maximum attainable value of C_t
C_T	wing thrust coefficient
K_T	thrust factor
$(L/D)_{max}$	maximum lift-to-drag ratio
M	Mach number
M_N	component of Mach number normal to wing leading edge = $M(1 + \sin^2\alpha \tan^2\Lambda)^{1/2} \cos \Lambda$
R_e	Reynolds number
r	wing section leading-edge radius
t	wing section maximum thickness
x,y,z	Cartesian coordinates
y_{le}	y coordinate of wing leading edge
z_{le}	z coordinates of wing section leading edge
z_{te}	z coordinates of wing section trailing edge
Δz	$z_{le} - z_{te}$
α	angle of attack
α_N	angle of attack normal to wing leading edge = $\tan^{-1}(\tan\alpha/\cos\Lambda)$
α_{SEP}	angle of attack at which separation occurs
β	$\sqrt{M^2-1}$
δ_f	leading-edge flap deflection angle
Λ	wing leading-edge sweep angle
η	fraction of local wing semi-span
η_v	location of vortex-action point

Introduction

For the last 20 years, a considerable effort has been directed toward the design of aerodynamically efficient wings for supersonic aircraft. During the first 15 years, the efforts were directed at transport-type aircraft. For these small-disturbance-producing aircraft, linearized-theory, zero-thrust, attached-flow optimization procedures[1,2] were extremely successful in producing efficient twisted and cambered wing designs.[3,4] These wings were characterized by low wing loadings and sharp leading edges. The low wing loading made it possible to produce wing designs within the limits of subcritical flow; thus, these designs remained well within the applicable range of linearized theory and avoided drag problems associated with separated flow and shocks. The purpose of the sharp leading edge was to reduce wave drag.

In the late 1970's, studies[5] indicated that future requirements of military aircraft would include efficient supersonic cruise and maneuver capabilities. Several studies have attempted, with varying degrees of success, to apply the linearized-theory wing-design methodology to the fighter wing-design problem,[6,7] however, studies have also been directed at applying nonlinear-flow phenomena to this wing-design problem. These latter efforts have been enhanced by recent advances in the understanding of and in the prediction of nonlinear flows--specifically, leading-edge thrust, supercritical crossflow, and separated leading-edge vortex flow. The purpose of this paper is to review and summarize the results of these supersonic wing-design studies which have employed nonlinear flows.

Discussion

The three nonlinear flow phenomena to be discussed are leading-edge thrust, supercritical crossflow, and leading-edge vortex flow. Leading-edge thrust is primarily a subcritical attached-flow phenomena, and is, therefore, applicable to the design of wings required to produce moderate or cruise levels of lift. Supercritical crossflow and leading-edge vortex flow are, respectively, attached-flow and separated-flow concepts seen as applicable for the design of wings to produce low levels of drag-due-to-lift at high-lift conditions. The two attached-flow concepts have received the most attention, are the best understood, and will be discussed first followed by a discussion of the separated leading-edge vortex flow concept.

Leading-Edge Thrust

The existence of leading-edge thrust on highly swept wings at supersonic speeds has been known for some time;[8,9] however, typical supersonic wings with thin airfoils and rather sharp leading edges fail to produce any significant amount of the theoretical thrust. As a result, leading-edge thrust has been virtually ignored in the design and analysis of supersonic wings and, in fact, widely used supersonic wing-camber design and optimization procedures[2] use loadings which preclude the attainment of any leading-edge thrust.

Recent developments in supersonic wing research have produced methods for predicting both theoretical[10] and attainable[11] levels of leading-edge thrust; these methods have been implemented in a computer code described in reference 12. Using results from these methods, thrust producing wings were reported[13,14] to offer some significant theoretical benefits over conventionally designed zero-thrust wings. With this impetus, an experimental and theoretical study was performed to examine the effects of planform shape and leading-edge radius on the leading-edge thrust characteristics. Most recently, a computer code has been assembled which includes attainable thrust in the camber surface optimization.[15] The remaining discussion in this section will review the thrust prediction methodology, summarize results of the experimental study, and present an example illustrating the optimization procedure.

The essential elements of the reference 11 method for calculating attainable levels of leading-edge thrust are presented in figure 1, where an uncambered airfoil is used for discussion purposes. The attainable thrust definition makes use of an empirical thrust factor, K_T, which is the fraction of full thrust (as calculated in ref. 10) actually produced as an attached-flow, airfoil nose force in the thrusting direction. Values of K_T less than unity indicate the presence of a leading-edge vortex force which, according to the Polhamus suction analogy,[8] acts in a direction normal to the thrusting direction. The thrust factor, K_T, can have values ranging from unity for fully attached flow to values of zero for completely separated flow. In general, the thrust factor will vary along the wing leading edge and, as indicated in figure 1, depends on the leading-edge sweep and radius, the inviscid loading, and the free-stream values of Mach number and Reynolds number.

Because little attention has been given to supersonic cruise configurations with rounded leading edges, it is difficult to find data which display appreciable amounts of leading-edge thrust. A few examples are given in reference 16. Unpublished data shown in figure 2 serve to demonstrate, rather clearly, a significant amount of thrust for Mach numbers up to 2.95. An axial or chord force coefficient plotted as a function of angle of attack is the best indicator of the presence or absence of leading-edge thrust. All calculated results shown in figure 2 are solutions which can be obtained from the computer code described in reference 12. Linearized theory with no leading-edge thrust predicts no variation of axial force with angle of attack; however, the nonlinear aerodynamic code of reference 12 predicts a small decrease in zero-thrust axial force (long dashed line) due to a compressibility-type correction applied to the linearized-theory surface pressures. When the full thrust is included (the short dashed line), a large decrease in axial force is predicted. More important, however, is the effect due to attainable thrust. The attainable-thrust estimate is seen to agree well with the experimental data. For this wing with a 5-percent thick section, more than half of the full theoretical thrust is realized for angles of attack as high as 4°.

The prediction method was next used to study the influence of planform shape and leading-edge radius on attainable thrust. An example with wing planform as the variable is shown in figure 3. A complex wing planform[13,14] (results given by solid line) is compared with three other planforms all having the same span, overall length, trailing-edge shape, leading-edge radius, and maximum thickness with respect to the leading edge. Two of the comparison planforms have straight leading edges with sweeps of 66.6° and 68.8°; the third planform is identical to the complex planform except for the straight, 66°-swept leading edge outboard of 48-percent span. Although the study reported in reference 14 indicates that the complex planform would produce significant amounts of leading-edge thrust, the results at the left of the figure indicate that possibly less complex planforms would produce even more attainable thrust over a wide range of lift coefficients. As shown by the spanwise thrust distributions in the right of the figure, the constant-sweep planforms do not produce as much thrust inboard but do not lose as much outboard; therefore, both constant-sweep planforms are overall better thrust producers than the original complex planform.

An example with leading-edge radius as the variable is shown in figure 4. The wing has a 70° swept leading-edge planform with a 3-percent circular arc basic airfoil and is operating at a Mach number of 2 and a Reynolds number of 200 million. The leading-edge radius variation was obtained by replacing the basic sharp airfoil with parabolic nose sections to provide a series of three different leading-edge radii corresponding to r/t values of 0.0, 0.015, and 0.030. Drag due to lift was predicted with full thrust and with attainable thrust using the computer code of reference 12; the zero-lift wave drag was predicted using the far-field wave-drag method of

reference 17. At the left of the figure, the lift-drag polars show that the attainable thrust provided by increasing the leading-edge radius does indeed reduce the drag in the direction of the full-thrust drag estimate. The zero-lift drag values, which are indistinguishable in the plot, are tabulated on the figure and indicate only a 6-percent increase when r/t is increased from 0.0 to 0.030. The results shown at the right of the figure indicate that an appreciable increase in the maximum lift-drag ratio can be obtained for relatively small changes in leading-edge radius.

Because wing planform and leading-edge radius had been found to have such a dramatic effect on leading-edge thrust, a study was conducted to investigate the possibility of using attainable leading-edge thrust as a guide for designing efficient wing leading-edge shapes which would have good thrust-producing, attached-flow characteristics. A wind-tunnel model was defined by first selecting a planform which had desirable leading-edge thrust characteristics for a constant leading-edge radius to chord ratio, r/c. Then, three r/c distributions were chosen to produce different thrust characteristics. A very extensive theoretical aerodynamic examination of planform shapes and leading-edge radii distributions was performed[18] for a Mach number of 1.8 and a Reynolds number per foot of 2 million. Characteristics of the final selections of planform and leading-edge radius are shown in figures 5 and 6. Figure 5 shows characteristics of the initial (ref. 13) and final planforms. In general, it was found that the more gradual sweepback variation (variation in $\beta \cot \Lambda$) produced the most desirable leading-edge thrust distribution. The final planform selection has a much smoother thrust factor variation, and at $\alpha = 6°$ the separation onset location (point where K_T departs from 1.0) has been improved by moving it outboard. Figure 6 shows characteristics of the three leading-edge radii distributions in which the basic airfoil shape (NACA 65A004) was modified ahead of the 25-percent chord position. Corresponding most closely to the standard NACA 65A004 standard airfoil section, the baseline leading edge had a constant r/c value of 0.001 across the entire wing span. Another leading-edge geometry varied spanwise from an r/c value of 0.001 at the 10-percent span station to a maximum value of 0.004 at 30 percent and gradually decreased to an r/c value of 0.00225 at the tip. The third leading-edge geometry was sharp with r/c varying from 0.001 at the 10-percent span station to a value very near zero at the 20-percent span station. In the lower portion of the figure, the separation and thrust characteristics are shown to be quite different for the different leading-edge radii. The separation location (where K_T departs from unity) for the varying r/c is slightly better than the 0.001 r/c, and both of these are far superior to the sharp leading edge. The thrust characteristics (C_t plot) show the potential for producing leading-edge thrust is essentially zero for the sharp leading-edge radius and much better for the varying r/c than the constant 0.001 r/c.

The wind-tunnel model consisted of a main wing with minimum fuselage to house the sting and balance. As shown in figure 7, the model had interchangeable leading edges and was instrumented for measuring both forces and surface pressures. Experimental force and pressure data[19] were obtained for a Reynolds number per foot of 2 million at Mach numbers of 1.6, 1.8, 2.16, and 2.36. These results can be summarized with the aid of figures 8 and 9. In figure 8, typical experimental and theoretical axial-force results are shown at Mach numbers of 1.80 and 2.36 for the three different leading-edge radii. For both the high and low Mach numbers, the theory predicts that the sharp-, the 0.001-, and the varying-r/c wings produce respectively increasing amounts of leading-edge thrusts. Also, theoretically the level of thrust is larger and the effect of leading-edge radius on thrust is more pronounced at the lower Mach number. The experimental data indicate a somewhat different situation. At a Mach number of 1.8, the lower angle-of-attack thrust forces increase with decreasing leading-edge radius; this is exactly opposite from the predicted results. At approximately 8° angle of attack, the axial-force data merge and cross over so that the thrust forces reverse their previous trend and now increase with increasing leading-edge radius. At the higher Mach number, the level of the experimental and predicted thrust is in much better agreement than for the lower Mach number; but below 14° angle of attack, the thrust dependence on leading-edge radius is again opposite to that predicted. Although these effects are not well understood, a thorough examination of the wing pressures[19] indicate that obserserved effects of leading-edge radii on axial force are indeed a result in changes in local leading-edge pressures. By examining the surface pressures in the vicinity of the leading-edge, it was also possible to extract the spanwise location of separation for various angles of attack. These results are shown in figure 9 along with predicted values determined by the condition when the thrust factor, K_T, breaks away from unity. As shown in the figure, the agreement between experiment and theory is very good. The sharp leading-edge wing exhibits separated flow across the entire span at $\alpha = 1°$ while both the other leading edges have an orderly development of separation beginning outboard and moving inboard with increasing angle of attack.

Because wing leading-edge shape (sweep, radius, and camber) has such a significant impact on the potential to produce thrust and because it has been shown that more practical and less severe camber surfaces are needed when leading-edge thrust forces are appreciable,[20] a method has been developed for including attainable leading-edge thrust in the camber optimization of wings at both subsonic and supersonic speeds.[15] This method uses a technique based on optimizing a set of candidate camber surfaces and differs from the previous methods[2] which were based on optimizing a set of wing loadings.

The effects of including attainable thrust in the wing-design procedure is illustrated in figure 10 by an example taken from reference 15. Three different approaches were employed to design a camber surface for a 70° leading-edge sweep, clipped, delta wing to produce a cruise-lift coefficient of 0.16 at a Mach number of 1.6 and a Reynolds number of 50 million (based on the mean geometric chord). Two of the design approaches employ a sharp leading-edge wing for the purpose of excluding leading-edge thrust in the camber design; the third design approach employs a round

leading edge for the purpose of including attainable thrust in the camber design. For one of the sharp-leading edge designs, a camber surface was optimized for the cruise-lift coefficient of 0.16 and for the other sharp leading edge for a reduced-lift coefficient of 0.12; the reduced-lift design produces less camber than the cruise-lift design and has been shown in previous studies to experimentally provide the better aerodynamic performance. A camber surface for the round leading-edge design was produced for cruise lift only.

The severity of wing warp for the three designs is shown across the upper part of figure 10 as spanwise distributions of wing twist $\Delta z/C_r$ at the cruise-lift orientation. The sharp leading-edge cruise-lift design has the most severely twisted surface while the other two designs have comparable amounts of twist. Theoretical drag-due-to-lift polars for each of the three designs are shown across the bottom of the figure. Both no-thrust and attainable-thrust results are shown for each of the three designs. The no-thrust results were obtained by analyzing the camber surfaces with sharp (r/c = 0) airfoil sections and the attainable-thrust results were obtained by using round (r/c = 0.001) airfoil sections. At zero lift, the round leading-edge design has the lowest drag and the sharp leading-edge cruise-lift design has the highest drag which again indicates that these have the least and the most severely warped surfaces, respectively. At the cruise-lift conditions of C_L = 0.16, the effect of including attainable thrust in the analysis is illustrated by comparing the no-thrust and the attainable-thrust results for each camber surface. The presence of thrust is indicated by a reduced drag and is seen to be most significant for the round leading-edge design and least significant for the sharp leading-edge cruise-camber design. The sharp leading-edge reduced camber design produces no thrust at the design-lift coefficient and only a slight amount of thrust at the higher cruise-lift condition. The most significant result from this example is found by examining the attainable-thrust drag polars along with the corresponding camber surfaces. The round leading-edge design has less drag due to lift at cruise lift than either of the other designs, and it has no more surface warping than the reduced camber design. Thus, a small amount of leading-edge radii to provide attainable leading-edge thrust produces the best overall camber design.

Supercritical Crossflow

One concept which has been shown to successfully produce high lift and low drag due to lift employs the use of attached supercritical crossflow. The essential considerations of the concept are shown in figure 11. Spanwise inviscid pressure distributions are illustrated at the left for a typical uncambered wing and at the right for a properly designed wing. When uncambered wings produce high lift, the inviscid pressure distributions generally have large expansion pressure peaks at the leading edge and large crossflow shocks when the flow decelerates to subcritical conditions. Either of these large pressure gradients would likely cause the real viscous flow to separate and they should, therefore, be avoided. The wing-design procedure would thus involve thickness and camber modifications to produce a pressure distribution with the characteristics shown on the right side of the figure. In this pressure distribution, the flow also accelerates to supercritical conditions but the absence of the large pressure gradients should be noted. The wing-design procedure results in the selection of a wing geometry which will produce a pressure distribution similar to that shown on the right portion of figure 11.

The theoretical-experimental study was conducted in two parts. The first part involved the design, analysis, and testing of a conical wing, and the second part involved a more practical fully three-dimensional wing. Although the conical wing geometry is realistically and aerodynamically impractical, it is the two-dimensional supersonic equivalent to a subsonic two-dimensional airfoil study which usually precedes a fully three-dimensional design. Likewise, the purpose of the conical-wing study was only to demonstrate the feasibility of obtaining the desired wing leading-edge flow conditions. A full-potential flow code[21] capable of accurately and efficiently analyzing highly nonlinear supersonic flows with embedded crossflow shocks was used to design the conical wing by iteration; no direct design method existed. Wind-tunnel models of a cambered wing and a comparison flat wing, with the same thickness distributions as the cambered wing, were designed and constructed. The models were instrumented to measure both force and surface pressures. A photograph of the cambered-wing wind-tunnel model is shown in figure 12; details of the design and testing can be found in reference 22.

The cambered conical wing was designed at a Mach number of 1.62 for a pressure distribution which would produce a lift coefficient of approximately 0.45 at 10° angle of attack and which would have no leading-edge expansion pressure peak and no recompression crossflow shock. The cambered-wing results in figure 13 show clearly that the theoretical pressure distribution was achieved experimentally. For approximately the same level of lift, the flat-wing pressure distribution exhibits a much larger leading-edge expansion followed by a strong recompression. These flat-wing pressure results are obviously less desirable than the cambered-wing results, and the flat wing did produce considerably more drag than the cambered wing at the design-lift condition.[22]

Having shown that it was possible to produce the desired supercritical crossflow in the context of two-dimensional conical flow, the second part of the study was to duplicate this achievement on a more practical, nonconical, typical fighter-type wing. Again, the design was an iterative analysis procedure using the fully three-dimensional potential-flow code of reference 23. Details of the design process, fabrication, and testing are presented in reference 24. The goal was to employ the shockless supercritical crossflow concept to meet the design conditions of C_L = 0.4 at M = 1.62. The wind-tunnel model was instrumented for measuring both forces and pressures as shown in the photograph of figure 14. A typical spanwise pressure distribution is shown in figure 15 for the design conditions of $\alpha = 12°$ and $C_L \approx 0.4$.

The experimental data confirm the nonlinear, potential, design-goal pressure distribution. The experimentally measured and theoretically predicted drag polars are shown in figure 16 along with the generally accepted linearized-theory upper (flat plate) and lower (zero-thrust optimum) boundaries. The measured and predicted results are in very good agreement. When compared with the linearized-theory boundaries, the wing is found to attain 52 percent of the theoretically available drag reduction. This proven capability to design a wing for high lift without excessive drag represents a significant advancement in the state-of-the-art for supersonic wing design. However, it should be noted that the wing design produced in this study only employed the concept of reducing drag by avoiding flow characteristics known to produce drag; perhaps an optimization technique such as that described in reference 25 would result in further drag reductions.

Leading-Edge Vortex Flows

The second approach to be considered for producing efficient high lift uses a controlled, separated, leading-edge vortex flow which not only produces vortex lift but when the vortex is located on the proper leading-edge shape also produces significant levels of effective leading-edge thrust. As summarized in reference 26, investigations at subsonic and transonic speeds of the fundamental vortex behavior on the leeward surface of wings have led to the design of several unique leading-edge devices referred to as "vortex flaps." Also, to aid in the design of low-speed vortex flaps, several computer codes[27 29] with varying degrees of complexity are being developed to predict vortex strength, location, and effect on the wing.

Recently, studies have been conducted to investigate the possibility of applying this concept at supersonic speeds. Although the major emphasis has been on understanding the fundamental vortex flows about flat delta wings,[30] computer codes to treat cambered wings of arbitrary planforms have been developed,[12 28] evaluated,[31] and applied to the design of a supersonic vortex flap. The principal findings of these studies will be presented in the remainder of this section. In supersonic flow, it is well known that at most moderate angles of attack, an uncambered wing with a highly-swept (subsonic), sharp leading edge will develop separated flow which results in a classical leading-edge vortex with the characteristics shown in figure 17. As the flow attempts to expand around a sharp leading edge, it separates and forms a region of rotational flow known as the "primary vortex." The highly rotational primary vortex induces velocities which can decrease the wing pressure distribution and produce vortex lift. In the classical situation, the primary vortex is above the wing and induces flow which reattaches at a point where there is streamwise flow on the inboard side of this point and outward spanwise flow on the outboard side. The outward spanwise flow can separate into a secondary vortex and create additional lift as illustrated by the shaded area in the pressure distribution of figure 17.

In order to design wings for aerodynamic efficiency using leading-edge vortex flows, it is necessary to know under what conditions a vortex will exist and at what conditions a vortex will have the potential for improving aerodynamic performance; in other words, it is necessary to define a design space. In the following discussion, a method is outlined for defining the design space for delta wings and an example is given of the design space for a delta wing producing a lift coefficient of 0.4.

In reference 30, a chart as shown in figure 18 was presented where delta-wing flow types were classified in terms of conditions normal to the leading edge; specifically, normal angle of attack (α_N) and normal Mach number (M_N). This chart indicates that six distinctly different types of flow can be produced by a delta wing at angle of attack. As shown in the figure, a classical vortex will exist for flow conditions corresponding to the $\alpha_N - M_N$ values which lie within the shaded region. The design space must lie within this region. Furthermore, conditions at which a vortex has the potential to improve aerodynamic performance can be determined by examining the division of lift between the upper and lower wing surface and by postulating a rather simple but reasonable restriction on this division of lift. In reference 31, it was shown for delta wings that there is a highly nonlinear shifting of lift from upper-surface vortex lift to lower-surface compression lift with increasing Mach number and increasing angle of attack. Figures 19 and 20 illustrate respectively the upper- and lower-surface normal-force behavior for flat delta wings with sharp, subsonic leading edges. The data in the figures represent leading-edge sweep angles from 58° to 85° and Mach numbers from 1.5 to 3.5.

As shown in figure 19, when the upper-surface normal force ($C_{N,U}$) is plotted as a function of the parameter $\alpha_N \beta \cot \Lambda$, the data reduce to a family of constant Mach number curves, and the dramatic effect that Mach number has on the ability of the upper surface to produce normal force is clearly shown. For example, as the Mach number is increased from 1.5 to 2.0, the maximum upper-surface normal force is reduced by one half. This reduction in lift-producing capability is attributed to the inability of the upper-surface pressures to exceed the vacuum limit which becomes more restrictive with increasing Mach number.

The lower-surface normal-force characteristics of figure 20 are only a function of leading edge sweep angle and angle of attack, and unlike the upper-surface normal force, they are essentially independent of Mach number. In general, the lower-surface normal force increases nonlinearly with increasing angle of attack and this nonlinearity becomes more pronounced with increased leading-edge sweep.

The results of both figures 19 and 20 combine to show that the nonlinear shifting of lift from upper to lower surface with increasing angle of attack is most pronounced for highly-swept wings at low supersonic Mach numbers. Also, the data of these two figures can be used to further define the design space for vortex flows over delta wings.

In terms of α_N and M_N, the region in which a leading-edge vortex would be produced for sharp leading-edge delta wings was identified in figure 18. Using the normal-force information presented in figures 19 and 20 and some realistic constraints, the design space can be further defined. For reasons given in reference 31, a lower Mach number of 1.20 and a maximum leading-edge-sweep angle of 75° were imposed. Combinations of these two constraints define a lower boundary which reduces the design space by 37 percent. Next, an acceptable solution for a given total normal-force coefficient is defined by requiring that the upper-surface normal force be equal to or greater than that of the lower surface; i. e., $C_{N,U} \geq C_{N,L}$. This requirement is based on the simple premise that drag reduction using leading-edge vortex flows can only be accomplished at conditions when the upper surface has significant suction-force production capacity. Although the specific condition imposed here is rather arbitrary, it does satisfy this premise.

Using the Mach number and leading-edge-sweep restrictions and the normal-force requirement, the design space for a delta wing to produce a total lift coefficient of 0.40 is shown in figure 21. This space is bounded on the right by maximum leading-edge-sweep angle, on the left by the vortex existence criterion, on the bottom by minimum Mach number, and on the top by the normal-force distribution requirement. Also indicated on the figure is the direction that the design space would move for decreasing total normal force.

In reference 30, the aerodynamic analysis code of reference 12 was shown to provide reasonable estimates of both vortex strength and vortex location. The effect of angle of attack on vortex strength is shown in figure 22 by examining the pressure distributions and integrated pressures on the upper surface of a delta wing at M = 1.7. For three angles of attack, inset sketches of the spanwise pressure distributions used to obtain the upper-surface normal-force parameter, $\int_0^1 C_p/C_{p,v}\, d\eta$, are also shown. The difference between the theory-without-vortex values and either experimental or theory-with-vortex values represents respectively the experimental or theoretical vortex-induced increment. For the entire angle-of-attack range, the vortex accounts for approximately a 50-percent increase in the attached-flow normal force. In terms of the vortex increment, the theory underpredicts the experimental values by about 30 percent except at the largest angle of attack where the difference is less than 15 percent. The pressure distributions indicate that in the lower three-fourths of the angle-of-attack range, the theory predicts nearly the correct pressure distribution shape but, as reflected in the normal-force parameter, underestimates the pressure level. At the larger angles of attack, where the normal-force parameter is best predicted, the theoretical and experimental pressure distributions are in considerable disagreement. The effects of angle of attack, Mach number, and leading-edge sweep on vortex position are shown in figure 23. As shown in the sketch, the vortex position is identified by the location of the vortex-action point expressed as a fraction of the local wing span, η_v. The vortex-action point is the location at which the vortex normal-force vector should be placed to give the same moment as produced by the vortex-induced pressures. From the results shown in the figure, angle of attack has the largest effect on vortex position. Typically, the vortex-action point moves from a position near 80 percent of the semi-span to a location near 50 percent as angle of attack increases from 4° to 20°. According to the empirical relationship used in the prediction method of reference 12, there is no change in the vortex-action point with either leading-edge sweep or Mach number. Experimentally, only a very small inboard movement was observed with increased Mach number, and a small but inconstant variation was observed with change in leading-edge sweep. In general, the experimental vortex location is usually inboard of the theoretically-predicted location and the two agree within 10 percent.

The aerodynamic benefits theoretically offered by using vortex flaps at supersonic speeds are illustrated in figure 24. In this example, the effects of flap size and flap deflection on predicted drag due to lift are examined. Using the method of reference 12, aerodynamic characteristics were calculated for a series of three flat delta wings all having a leading-edge sweep of 75° and zero leading-edge radius. The three delta wings have conical leading-edge flaps which correspond in size to 10, 20, and 30 percent of the total wing area. Drag-due-to-lift values are presented for each of the wings for M = 1.8, C_L = 0.3 and for flap deflections varying from 0° to 30° (position δ_f leading edge down). For each of the flap sizes, there is a flap deflection which produced the minimum drag due to lift; these minimum-drag flap-deflection values increase as the flap size decreases. These results can be explained by examining the change in vortex strength and location. At the smaller flap deflections, the entire vortex is located on the flap and the vortex strength is small. As the flap is deflected and the wing angle of attack is increased to maintain a lift-coefficient value of 0.3, the vortex increases in strenth and moves aft on the flap. This behavior continues until the minimum-drag flap-deflection value is reached. At this point, a portion of the vortex begins to move behind the flap hinge line. This portion of the vortex which was on the flap producing effective thrust is now on the wing producing drag. Continued increasing flap deflection results in an increasing drag due to lift. For this example, the smallest flap produces the lowest drag due to lift which is shown to be 11 percent above the theoretical minimum 100-percent thrust value. This represents a significant reduction in drag due to lift when compared to the undeflected-flap value which is 51 percent above the theoretical minimum 100 percent thrust value. This example illustrates that a leading-edge vortex flap can theoretically provide significant drag reductions and that flap size and deflection effects are important.

Summary

Three nonlinear flow concepts for the design of supersonic wings have been reviewed. The specific concepts are: leading-edge thrust, supercritical crossflow, and leading-edge vortex flow.

The leading-edge thrust concept is viewed as

applicable to the design of wings for cruise levels of lift. Prediction methods which empirically account for attainable thrust levels are available for both the aerodynamic analysis and the camber design optimization of wings. The results of a theoretical and experimental study for selecting wing planform and leading-edge radius showed that the prediction method could be used to indicate the onset of leading-edge separation but that the prediction method was optimistic in estimating the thrust forces. Theoretically, results from a camber design-optimization example indicated that providing a small amount of leading-edge radius for thrust production will result in the following benefits: less severe and more realistic wing camber, essentially same level of aerodynamic performance as predicted for a zero-thrust full camber design, and less drag at off-design conditions. These theoretically predicted benefits must be experimentally verified.

The supercritical crossflow concept is applicable to the design of wings for maneuver levels of lift. A nonlinear full-potential flow code was used for aerodynamic analysis; however, design was accomplished by iterative analysis since no direct design or optimization capability exists. Two experimental-theoretical studies have been conducted in the development of the concept. In the first study, the concept was validated within the limited but simple conditions of conical flow. In the second study, the concept was demonstrated on a fully three-dimensional fighter-type wing. Further development of the concept will involve design-optimization and configuration integration.

The leading-edge vortex concept is another approach for the design of wings for maneuver levels of lift. The concept involves combining a separated leading-edge vortex-induced loading on a deflected leading-edge flap to obtain enhanced lift and effective thrust. Fundamental properties of leading-edge vortex flows have been studied for such flows about flat delta wings with sharp leading edges, and the results of these studies have been used to define conditions at which these flows will exist and to further define a design space in which vortex flows can be used to improve performance. An aerodynamic analysis method has also been shown to be effective in predicting the general properties of vortex flows about flat delta wings. However, similar studies have not been examined for wings with deflected flaps. Assuming that the flat delta wing findings will hold for deflected flaps, a theoretically generated example shows that significant drag reductions can be produced by proper selection of flap size and flap deflection. These theoretical predictions must be experimentally verified.

References

1. Carlson, Harry W., and Middleton, Wilbur D., A Numerical Method for the Design of Camber Surfaces of Supersonic Wings with Arbitrary Planforms. NASA TN D-2341, 1964.
2. Carlson, H. W.; and Miller, D. S.: Numerical Methods for the Design and Analysis of Wings at Supersonic Speeds. NASA TN D-7713, 1974.
3. Carlson, H. W.: Aerodynamic Characteristics at Mach Number 2.05 of a Series of Highly-Swept Arrow Wings Employing Various Degrees of Twist and Camber. NASA TM X-332, 1960.
4. Morris, O. A.; and Fournier, R. H.: Aerodynamic Characteristics at Mach Numbers 2.30, 2.60, and 2.96 of a Supersonic Transport Model Having a Fixed, Warped Wing. NASA TM X-1115, 1965.
5. Meyer, R. C.; and Fields, W. D.: Configuration Development of a Supersonic Cruise Strike-Fighter. AIAA Paper No. 78-148, 1978.
6. Shrout, B. L.; and Fournier, R. H.: Aerodynamic Characteristics of a Supersonic Cruise Airplane Configuration at Mach Numbers of 2.3, 2.96, and 3.3. NASA TM-78792, 1978.
7. Miller, D. S.; and Schemensky, R. T.: Design Study Results of a Supersonic Cruise Fighter Wing. AIAA Paper No. 79-0062, 1979.
8. Polhamus, E. C.: Drag Due to Lift at Mach Numbers up to 2.0. NACA RM-L53I22b, 1953.
9. Sotomayer, W. A.; and Weeks, T. M.: Application of a Computer Program System to the Analysis and Design of Supersonic Aircraft. AIAA Paper No. 77-1131, 1977.
10. Carlson, H. W.; and Mack, R. J.: Estimation of Leading-Edge Thrust for Supersonic Wings of Arbitrary Planform. NASA TP-1270, 1978.
11. Carlson, H. W.; Mack, R. J.; and Barger, R. L.: Estimation of Attainable Leading-Edge Thrust for Wings at Subsonic and Supersonic Speeds. NASA TP-1500, 1979.
12. Carlson, H. W.; and Mack, R. J.: Estimation of Wing Nonlinear Aerodynamic Characteristics at Supersonic Speeds. NASA TP-1718, 1980.
13. Robins, A. W.; Lamb, M.; and Miller, D. S.: Aerodynamic Characteristics at Mach Numbers of 1.5, 1.8, and 2.0 of a Blended Wing-Body Configuration With and Without Integral Canards. NASA TP-1427, 1979.
14. Robins, A. W.; and Carlson, H. W.: High-Performance Wings With Significant Leading-Edge Thrust at Supersonic Speeds. Journal of Aircraft, Vol. 17, June 1980, pp. 419-422.
15. Carlson, H. W.; Shrout, B. L.; and Darden, C. M.: Wing Design With Attainable Thrust Considerations. AIAA Paper No. 84-2194, 1984.
16. Puckett, A. E.; and Stewart, H. J.: Aerodynamic Performance of Delta Wings At Supersonic Speeds. Journal of Aeronautical Science, Vol. 14, No. 10, October 1947, pp. 567-587.
17. Harris, R. V., Jr.: An Analysis and Correlation of Aircraft Wave Drag. NASA TM X-947, 1964.
18. Middleton, W. D.: Study of Supersonic Wings Employing the Attainable Leading-Edge Thrust Concept. NASA CR-3637, 1982.
19. Wood, R. M.; and Miller, D. S.: Experimental Investigation of Leading-Edge Thrust at Supersonic Speeds. NASA TP-2204, 1983.
20. Carlson, H. W.; and Miller, D. S.: The Influence of Leading-Edge Thrust on Twisted and Cambered Wing Design for Supersonic Cruise. AIAA Paper No. 81-1656, 1981.
21. Mason, W. H.; and Rosen, B. S.: The COREL and W12SC3 Computer Programs for Supersonic Wing Design and Analysis. NASA CR-3676, 1983.
22. Miller, D. S.; Landrum, E. J.; Townsend, J. C.; and Mason, W. H.: Pressure and Force Data for a Flat Wing and a Warped Conical Wing Having a Shockless Recompression at Mach 1.62. NASA TP-1759, 1981.

23. Siclari, M. J.: The NCOREL Computer Program for 3D Nonlinear Supersonic Potential Flow Computations. NASA CR-3694, 1983.
24. Mason, W. H.: A Wing Concept for Supersonic Maneuvering. NASA CR-3763, 1983.
25. Aidala, P. V.; Davis, W. H., Jr.; and Mason, W. H.: Smart Aerodynamic Optimization. AIAA Paper No. 83-1363, July, 1983.
26. Lamar, J. E.; and Campbell, J. F.: Recent Studies at NASA-Langley of Vortical Flows Interacting with Neighboring Surfaces. AGARD Symposium on Vortical Type Flows in Three-Dimensions, Paper No. 10, 1983.
27. Johnson, F. T.; Lu, P.; Tinoco, E. N.; and Epton, M. A.: An Improved Panel Method for the Solution of Three-Dimensional Leading-Edge Vortex Flows. Volume I.- Theory Document. NASA CR-3278, 1980.
28. Lan, C. E.; and Chang, J. F.: VORCAM - A Computer Program for Calculating Vortex Lift Effect of Cambered Wings by the Suction Analogy. NASA CR-165800, 1981.
29. Lamar, J. E.; and Herbert, H. E.: Production Version of the Extended NASA-Langley Vortex Lattice FORTRAN Computer Program - Volume I - User's Guide. NASA TM-83303, 1982.
30. Miller, D. S.; and Wood, R. M.: An Investigation of Wing Leading-Edge Vortices at Supersonic Speeds. AIAA Paper No. 83-1816, July 1983.
31. Wood, R. M.; and Miller, D. S.: Assessment of Supersonic Wing Leading-Edge Vortex Prediction Techniques. AIAA Paper No. 84-2208, August 1984.

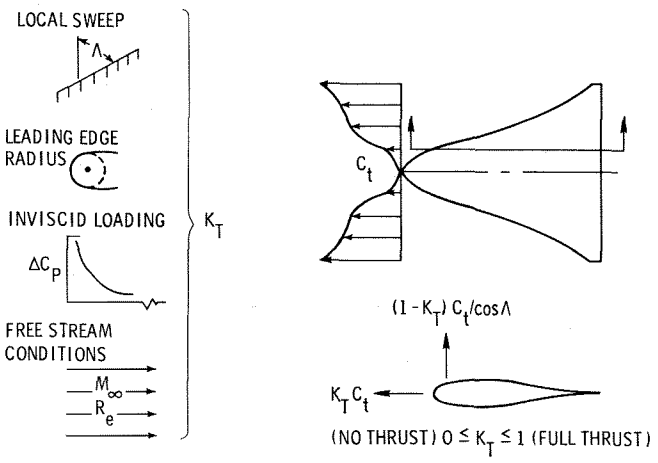

Figure 1. - Attainable leading-edge thrust concept.

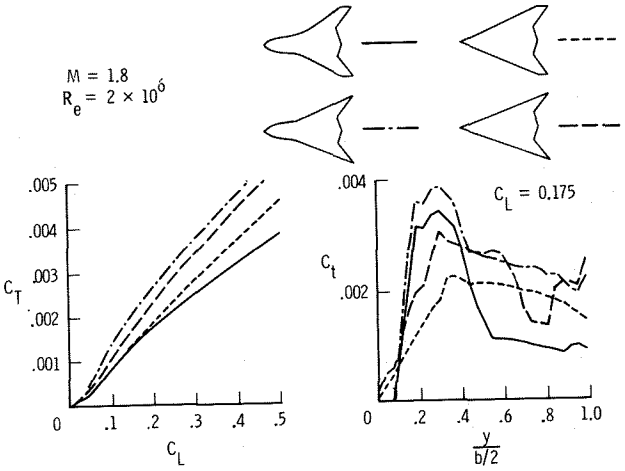

Figure 3. - Influence of planform on attainable leading-edge thrust.

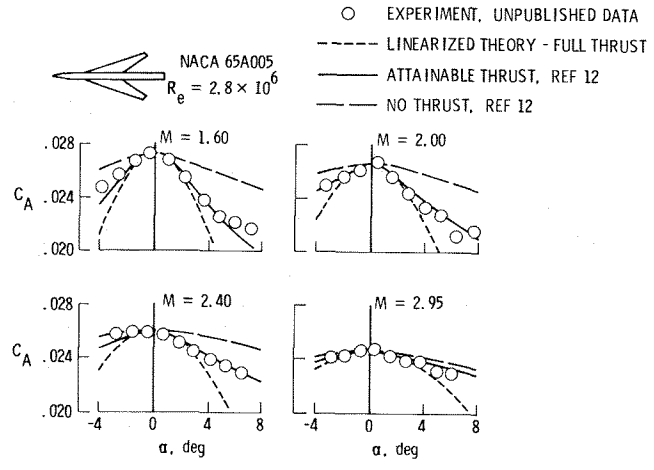

Figure 2. - Illustration of attainable leading-edge thrust.

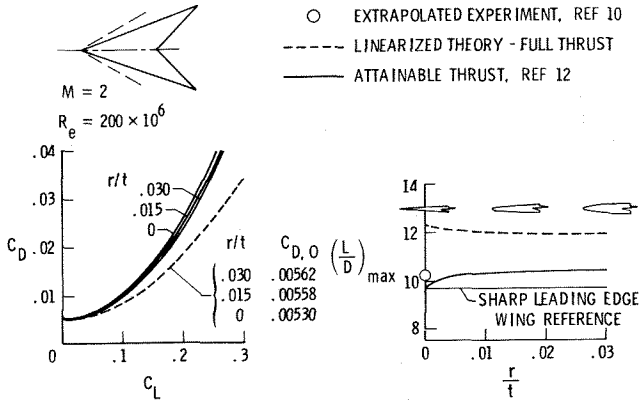

Figure 4. - Influence of leading-edge radius on attainable leading-edge thrust.

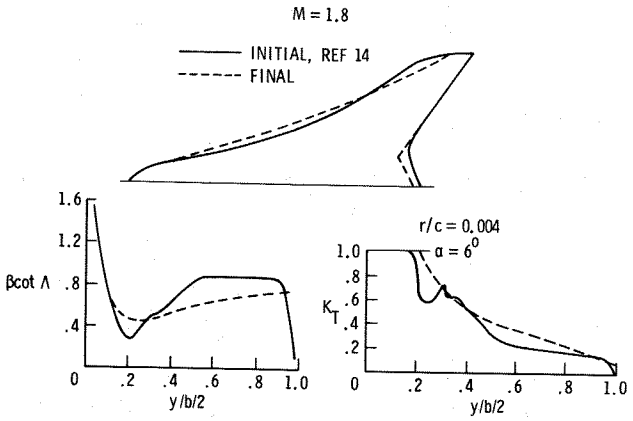

Figure 5. - Planform selection.

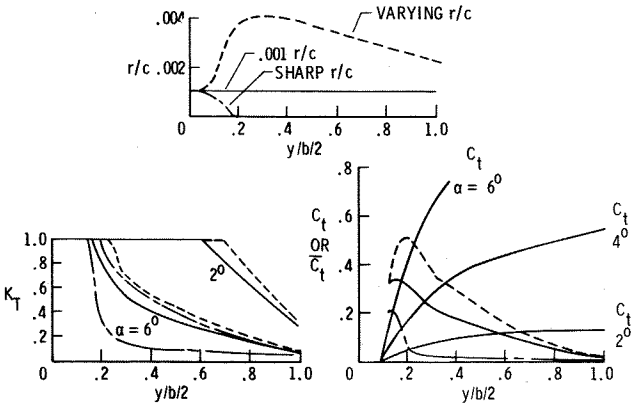

Figure 6. - Leading-edge radii selections.

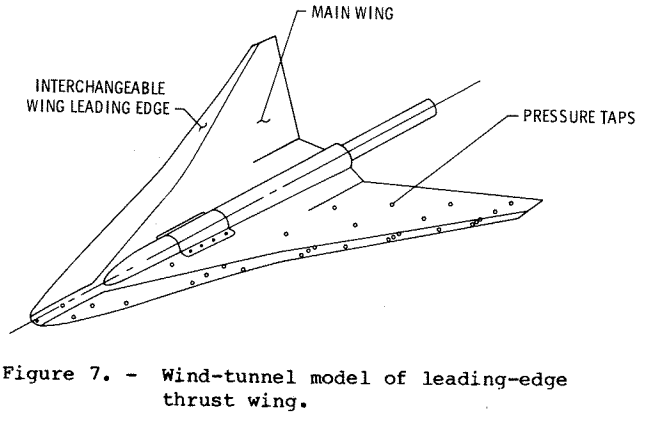

Figure 7. - Wind-tunnel model of leading-edge thrust wing.

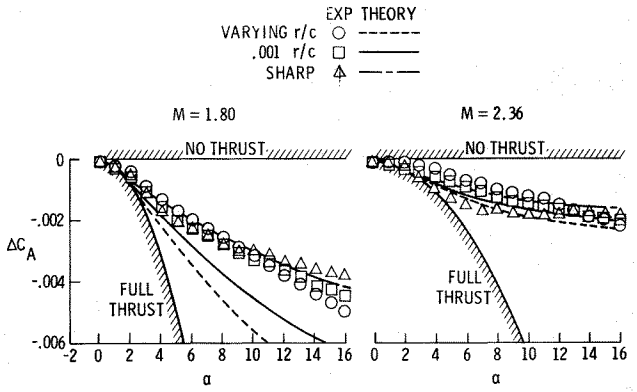

Figure 8. - Effect of leading-edge radius on axial force.

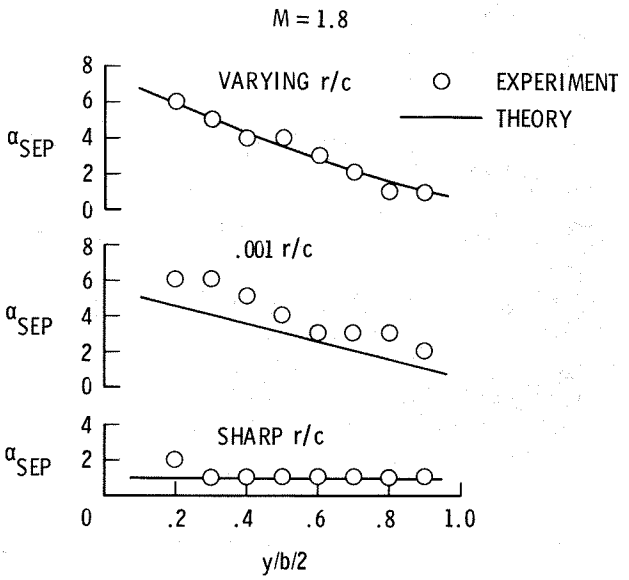

Figure 9. - Location of leading-edge flow separation.

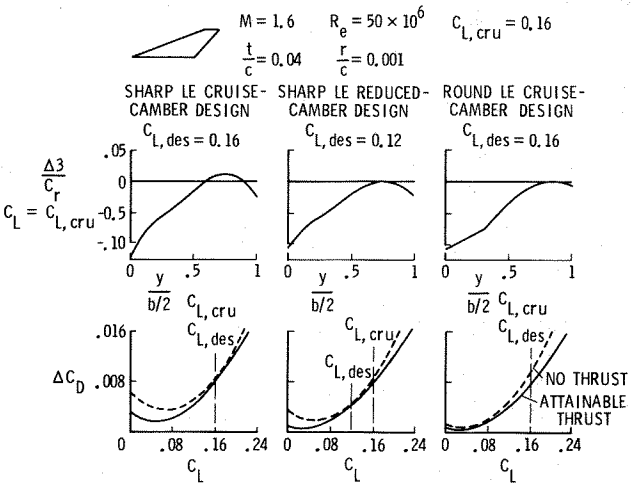

Figure 10. - Effect of including leading-edge thrust in wing camber optimization.

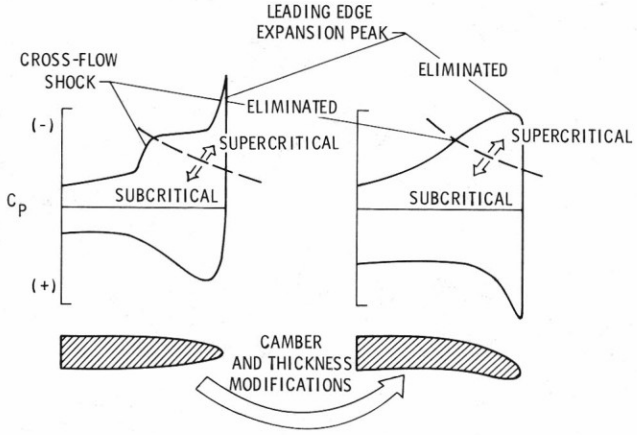

Figure 11. - Supercritical crossflow wing-design concept.

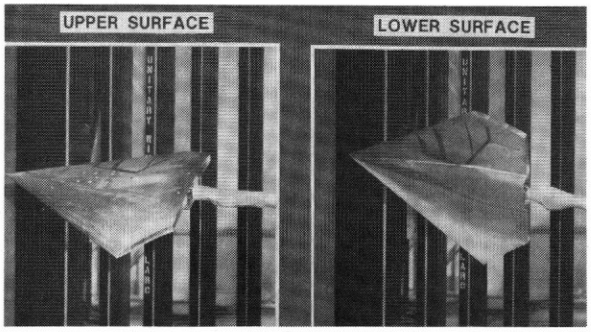

Figure 12. - Photograph of cambered conical-wing wind-tunnel model.

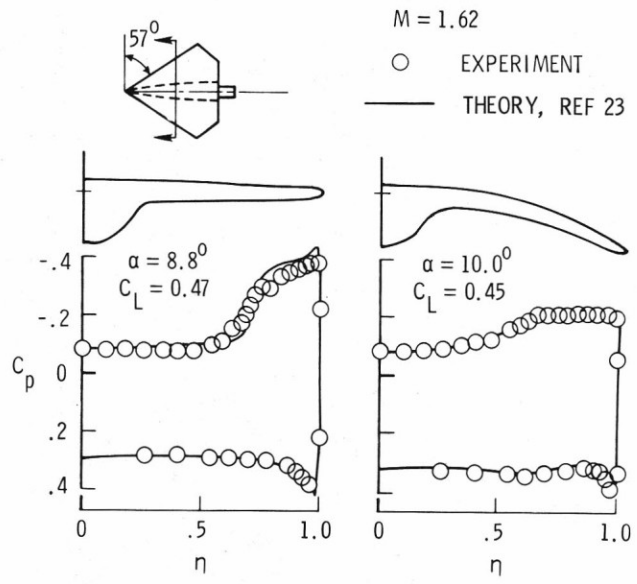

Figure 13. - Spanwise pressure distributions of conical wings.

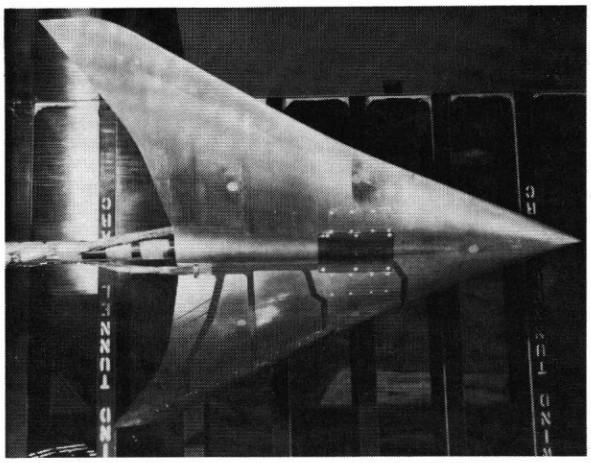

Figure 14. - Photograph of nonconical demonstration wing wind-tunnel model.

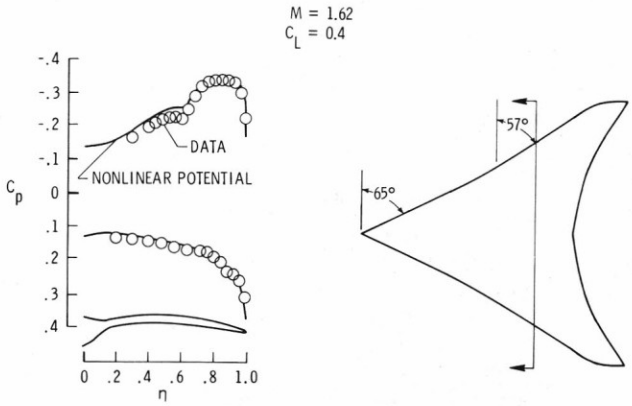

Figure 15. - Demonstration wing pressure results.

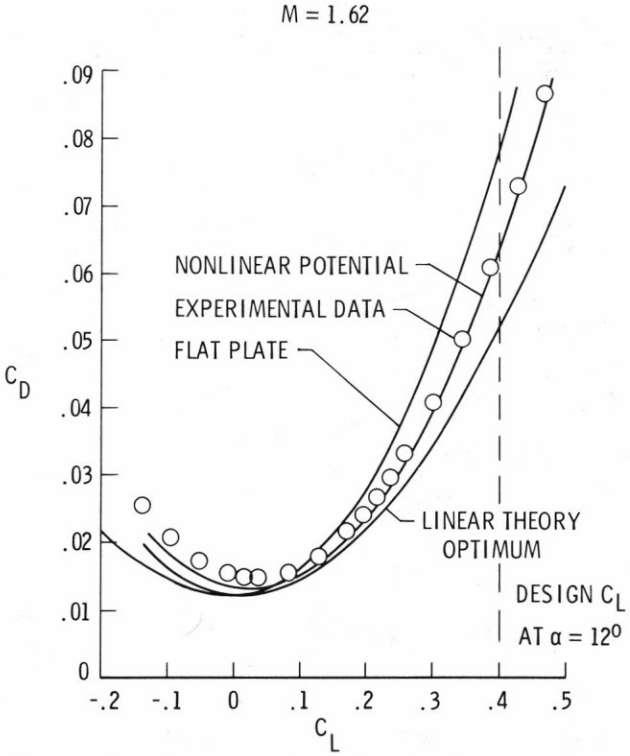

Figure 16. - Demonstration wing force results.

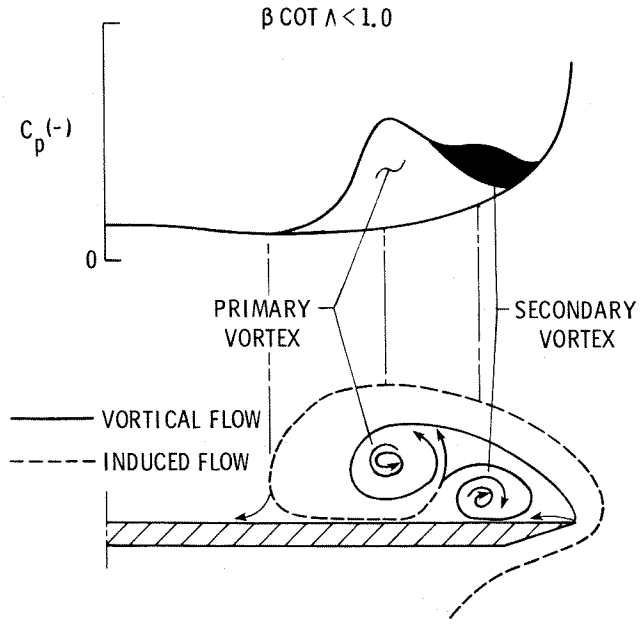

Figure 17. - Classical leading-edge vortex characteristics.

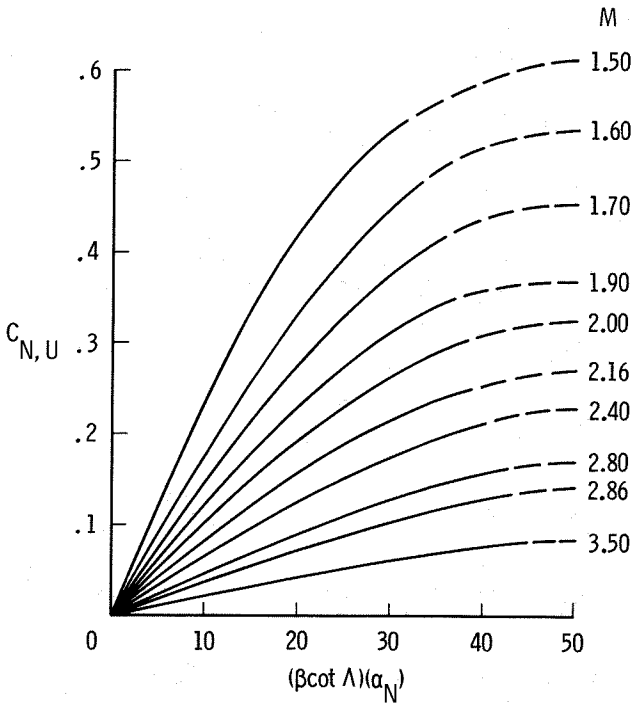

Figure 19. - Delta-wing upper-surface normal-force characteristics.

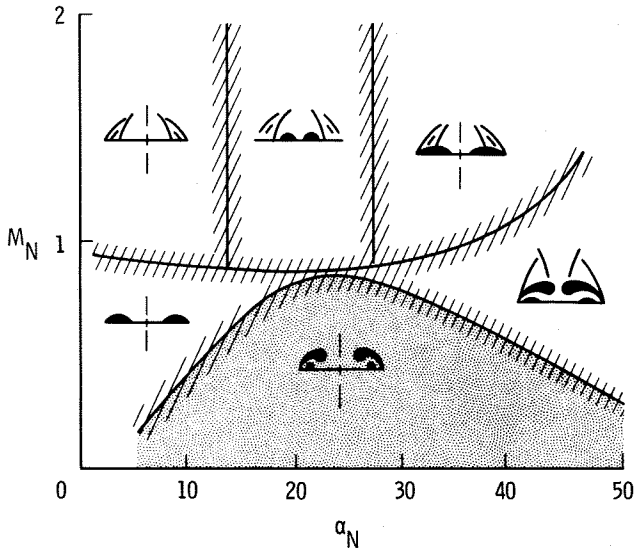

Figure 18. - Delta-wing leeside flow characteristics at supersonic speeds.

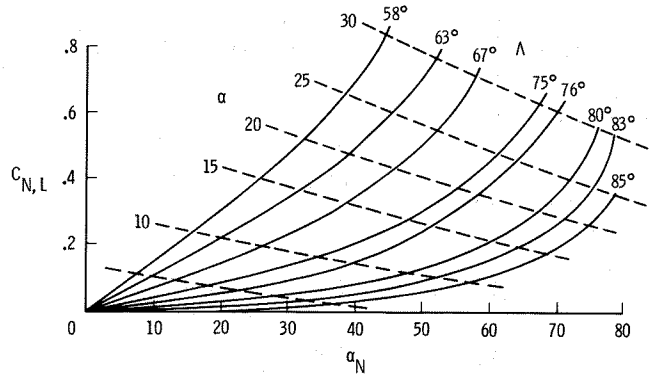

Figure 20. - Delta-wing lower-surface normal-force characteristics.

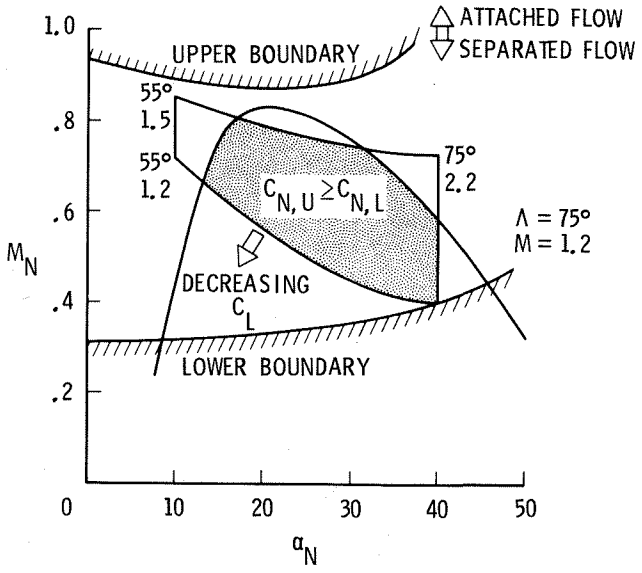

Figure 21. - Design space for leading-edge vortex flow on delta wing at $C_L = 0.4$.

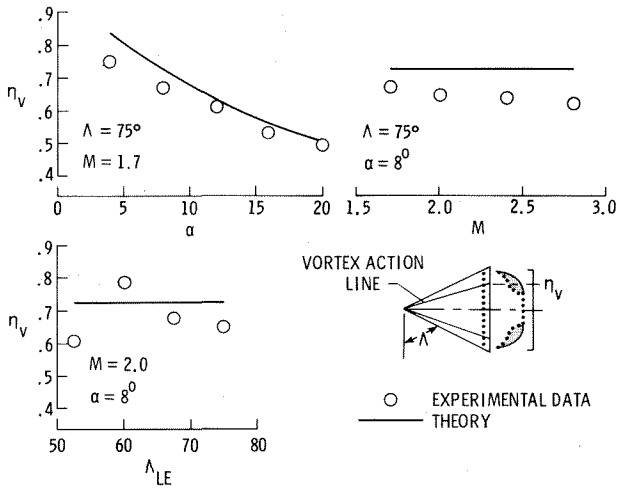

Figure 23. - Location of vortex action line for delta wings.

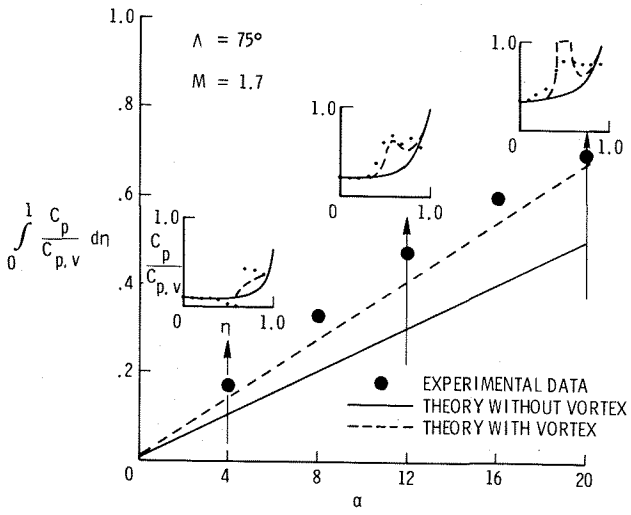

Figure 22. - Effect of angle of attack on vortex strength for delta wings.

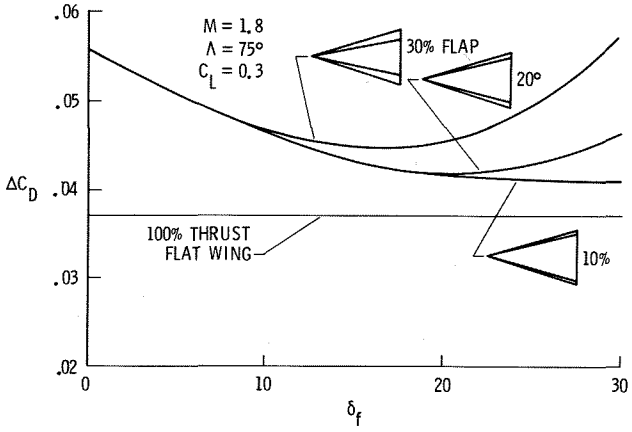

Figure 24. - Effect of leading-edge flap size and deflection on drag due to lift of delta wing.